

Turbine Design Report

Wildcat Wind Power
Kansas State University



2022 | 2023

Officer Team

Brianna Wagoner | President
Andy Freshnock | Vice President
Jacob Lowe | Mechanical Team Co Lead
Rebecca Semple | Mechanical Team Co Lead
Michael Brosseit | Electrical Team Co Lead
David Pierson | Electrical Team Co Lead
Israel Barraza | Siting Team Co Lead
Jakob Long | Siting Team Co Lead
Kent Deterding | Secretary
Macie Sexten | Treasurer

Contact

barrazab@ksu.edu
Carl R. Ice College of Engineering
1046 Rathbone Hall
1701B Platt St., Manhattan, KS 66506
785 532 560

Mechanical Team

Jose Rodriguez
Josh Meurer
Jacob Ronnekamp
Phillip Shirkey

Electrical Team

Cameron Million
Sidney Wagner
Parker Dawdy
David Ochner

Siting Team

Nick Saia
Rory Jenkins
Chase Classcock
Levi Francis

Contents

Executive Summary 2

Design Objectives..... 3

Knowledge From Past Competitions 3

Technical Design..... 4

 Foundation and Tower4

 Nacelle and Yaw5

 Active Pitch6

 Blade Design.....6

 Generator Selection9

 Turbine Side.....10

 Load Side11

 Electrical Systems Manufacturing..... 14

 Software 15

 State Machine Operation..... 16

Final Turbine Assembly19

 Assembly and Commissioning Checklist 20

References i

Executive Summary

Wildcat Wind Power at Kansas State University aimed to tackle the electrical, mechanical, and aerodynamic challenges set forth by the 2023 Collegiate Wind Competition. To this end, our team designed and fabricated a small-scale wind turbine system to be tested in a wind tunnel with a sea simulation tank. Our turbine, anchored to the simulation seabed, is designed to handle wind speeds up to 22m/s in a safe and reliable manner. This document takes an elemental approach to the design, construction, and testing process of our scaled offshore wind turbine system. Coupling mechanical and electrical control elements has allowed our team to assemble a system capable of meeting the requirements of the competition. Our final turbine for competition is pictured in Figure 1 below.

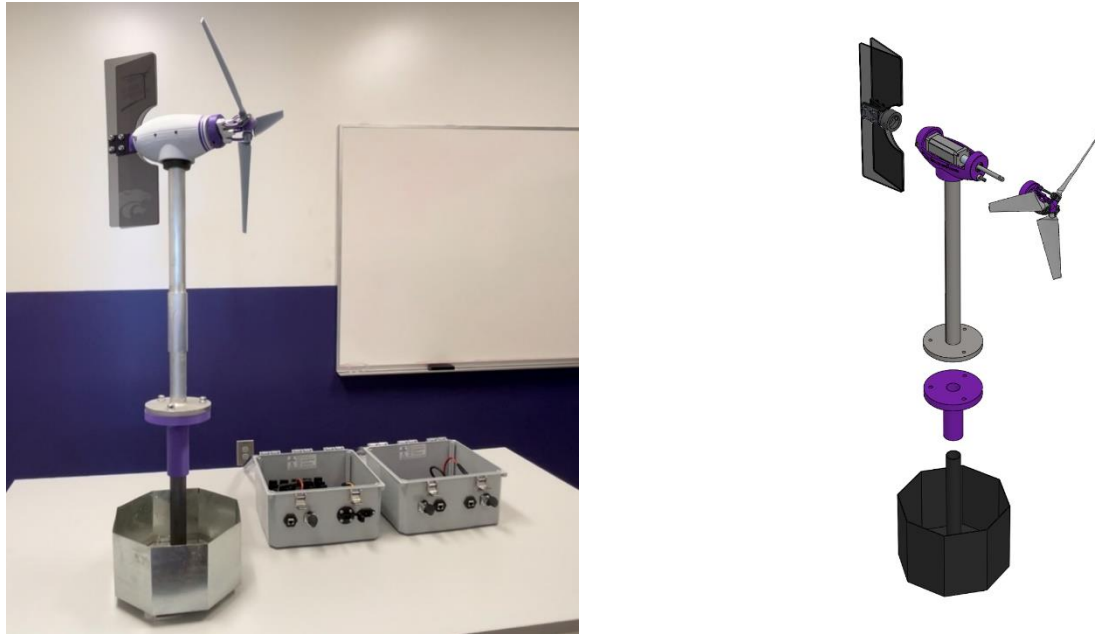


Figure 1: Full Turbine System (left) and 3D Exploded Assembly (right)

A strong foundation to anchor our turbine to the simulation seabed was of utmost priority. An octagonal prism that could be screwed into the sand was fabricated from plate and sheet steel. Moving upwards, at the top of the turbine assembly sits our 3D printed nacelle which houses our linear actuator and generator. This linear actuator powers the active pitch mechanism which provides our three blades over 100° of rotation for RPM control purposes. After over 45 design iterations, the optimal 3D printed blades were selected. The brushless DC generator, coupled to the rotor, converts rotational energy into electrical energy to be measured by the competition. Passive yaw allows our turbine to orient into the airflow through an acrylic tailfin mounted to the rear of the nacelle.

Our electrical system facilitates turbine operation as well as dissipates and controls power produced by the turbine. A Teensy 4.1 microcontroller mounted to our load-side board controls the system with information from sensors on both the load and turbine-side boards. For load optimization and power regulation, our team uses a DAC controlled, current sinking MOSFET load. To regulate RPM, our linear actuator is powered by a 7.4V buck converter and controlled by optically isolated, full-duplex serial communication with the load-side microcontroller. RPM is measured with the frequency of an optically isolated Hall-effect signal from the turbine-side board, and load voltage and current is measured with an INA260 IV sensor located on the load-side board.

Design Objectives

First and foremost, our team believes that the competition constraints and safety requirements should primarily inform our system's design objectives. After that, we believe the next most important objectives are those informed by the four turbine tasks.

- *Competition Safety and Technical Requirements*

Our turbine must fulfil certain safety and technical requirements laid out in the *Safety and Technical Inspection Sheet* to be deemed safe for competition. These requirements serve as a baseline for all design decisions.

- *Power Curve Performance Task Design Objective*

Efficiency of key power generation components is the main design consideration of this task. Due to the heavy emphasis on power generation in this task, the generator selection and blade design process are driven by the desire to maximize power during tested windspeeds.

- *Control of Rated Power and Rotor Speed Task Design Objective*

This task requires designing control mechanisms to precisely regulate both RPM and power during high wind speeds. The regulation of RPM is largely dependent on mechanical design while regulation of power is largely dependent on electrical design.

- *Safety Task Design Objective*

To complete the objective, our turbine must be able to rapidly shut down upon an open e-stop switch or a PCC discontinuity. Mechanical systems aim to physically shut down and reduce our turbine's RPM. Electrical systems must navigate the signal processing to initiate a shut down.

- *Durability and Foundation Success Tasks Design Objective*

The task requires mitigating mechanical stress under demanding tunnel conditions. Regulating RPM is necessary to keep rotor components within their operational limits. The foundation has stability at the forefront of design considerations. Weight is a secondary design consideration when feasible.

Knowledge From Past Competitions

Our team utilized knowledge gained from last year's competition for the design process of this year's system. A full list of ideas and designs utilized from previous years is as follows:

- *Foundation*

A box-shaped foundation design was very stable for us during last year's competition. This design was modified to conform to the no-excavation rule of this year's competition. A solid steel base plate with sheet metal walls remained the same for this year's competition.

- *Tower*

Our team entirely reused our aluminum tower from previous competitions. Utilizing a recycled tower allowed our team to focus manufacturing efforts elsewhere.

- *Active Pitch*

Last year, our team successfully designed and built an active pitch system. Because it was able to regulate RPM, the fundamental design mostly remained the same.

- *Sensors and Circuits*

The diode bridge rectifier, Pololu buck/boost converter, and LC filter on the turbine-side board remained mostly the same. Basic code and circuitry for interacting with our linear actuator, IV sensor, and Hall-Effect sensor from last year was also reused. Because of past effectiveness, our team saw no need to explore new designs.

- *Operational Modes*

Although this year's software structure is entirely new, many concepts from previous experience were used in the design process. This experience was especially useful during the design of our state machine. An understanding of how and when to transition between states enabled a more efficient design process.

Technical Design

Foundation and Tower

To design an anchor capable of keeping our entire turbine assembly stable while minimizing weight, our team took from past experience. Past competitions showed that the most effective anchors were ones that utilized the weight of the sand to their advantage. This led our team to again design a steel plate bottom anchor with side walls. However, to comply with the no-excavation rule, our team sought to create a screw out of the base plate of the foundation instead of manually filling the foundation with a shovel. For easy screw installation, a circular design was selected for the base plate. An early prototype of the foundation was made from a trashcan with slits cut in bottom to allow it to burrow into the seabed [Figure 2]. Proof of concept testing was conducted with the prototype, and it was decided to move forward with this design.

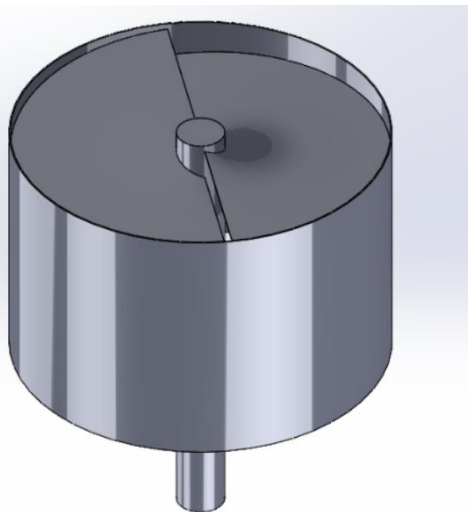


Figure 2: Initial Foundation Design 3D Rendering (Left) and Prototype (Right)

For easier manufacturing, it was decided that an octagonal base plate design was optimal. A waterjet was used to cut the perimeter of the baseplate and square spurs [Figure 3]. The spurs were then bent into place using a hydraulic press. After the baseplate was made, a 1.5" OD steel tube was metal inert gas (MIG) welded to the center of the baseplate to allow for the competition stub connection. Sheet metal was then bent and riveted to the baseplate to form the side walls of the anchor.

A T-shaped installation tool was manufactured from two steel tubes to provide leverage for rotating the foundation into the sand [Figure 3]. A 3D printed part mounts the two tubes perpendicular to one another. The installation tool slides over the foundation center tube and locks on using a retaining bolt.

To test our manufactured foundation, a recycled 35-gallon drum was cut in half to form a testing tank. This tank was then filled with sand and water to the competition specifications. Because we are unable to test the turbine in our wind tunnel while attached to the foundation, the completed foundation was tested separately in the tank using a spring scale, which determined it was stable to a torque of 34 Nm [Figure 3]. Calculations found the maximum torque our foundation will experience is 15 Nm. The weight of our final manufactured foundation is 6.94lbs.

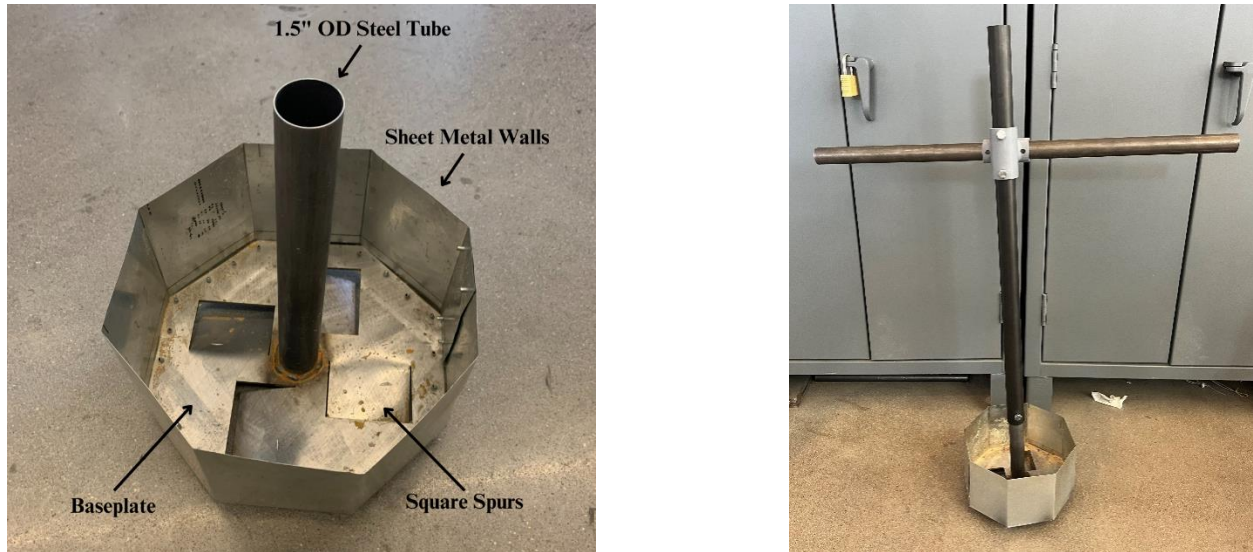


Figure 3: Manufactured Foundation (Left) and Installation Tool (Right)

Our aluminum tower, reused from last year, connects the competition stub piece to the nacelle. The tower features a press-fit bearing at the top to enable passive yaw.

Nacelle and Yaw

The geometry of the linear actuator, active pitch system, and generator primarily governed the 3D printed nacelle design. Our original nacelle design held two linear actuators on either side of the generator. To reduce power consumption, a single linear actuator design was adopted. Originally, we tested with the single linear actuator on the horizontal axis, but this placement resulted in a consistent yaw to one side. To prevent this, the linear actuator was moved to sit directly below the generator. This placement fixed the yawing issue and allowed for a narrower nacelle design [Figure 4].

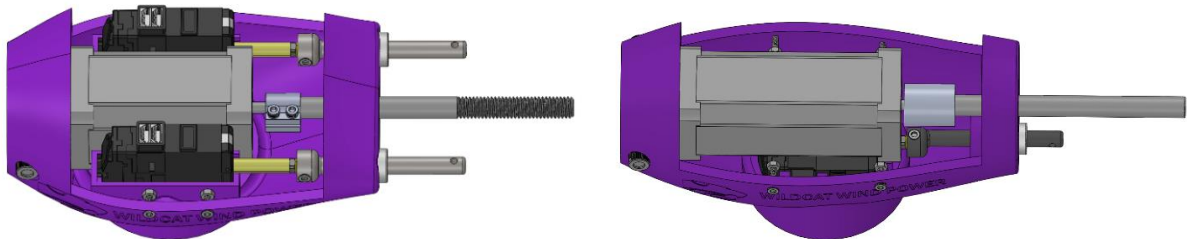
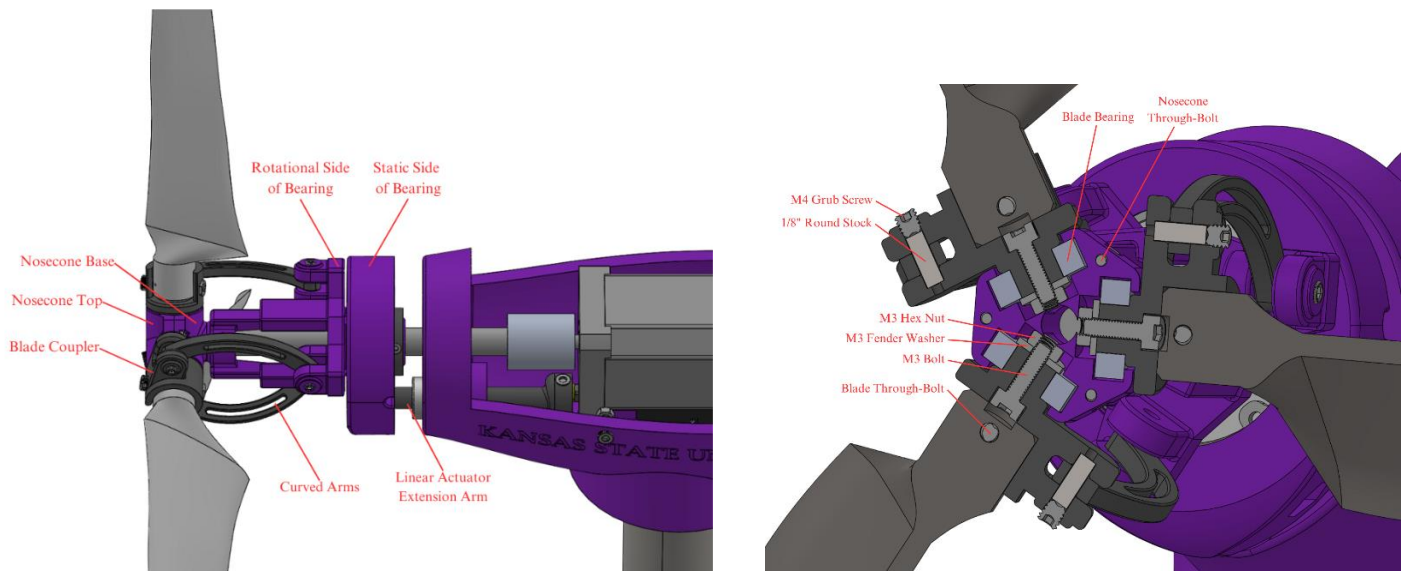


Figure 4: Dual Linear Actuator Nacelle Design (Left) and Single Linear Actuator Nacelle Design (Right)

The yaw system is comprised of two laser cut acrylic fins attached to the back of the nacelle and a press-fit bearing between the nacelle and turbine tower. The fins are connected to the nacelle with an angled 3D printed piece. These components allow for simple, passive yawing.

Active Pitch

The single linear actuator located within the nacelle controls the active pitch system. An extension arm allows the linear actuator to apply force to the static side of a bearing concentric with the rotating shaft. The static side of the bearing works to move the rotational side of the bearing horizontally as it rotates with the nosecone. Each of the three blades are secured to the nosecone via a blade coupler and bearing. The blade coupler is inserted into the bearing and secured with a M4 bolt. The two-piece nosecone encloses the bearings leaving the blades free to rotate. Three curved arms connect the blade couplers to the rotational side of the bearing. This connection allows the linear actuator to pitch the blades over 100 degrees. Aside from off-the-shelf bearing and pin joints, all individual components of the assembly were 3D-printed. The linear actuator to drive the system is a Progressive Automations PA-12 7.4V model which provides very high precision linear motion and performs well at all windspeeds. The active pitch has been tested up to 5,500 RPM but is regulated to 2,900 RPM during operation. A labelled SolidWorks model of the full final design, along with a diagram of the blade coupling and connection, is shown in Figure .



Blade Design

Our team chose to remain with a three bladed design for this year, as three bladed designs have a high theoretical maximum coefficient of performance (C_p), approximately 50%, compared the ultimate maximum Betz law, 59.3% [1]. A four bladed design was briefly considered as it has a higher max C_p , but three blades is inherently more stable and easier to balance. Additionally, a 4 bladed turbine would require more slender blades that would be more prone to bending.

The blades are optimized for a tip speed ratio (TSR) of six which offers the highest coefficient of power for a three bladed turbine. The chord lengths of the blades are calculated based on the TSR, induction factors, and coefficient of lift produced by the airfoils that make up the cross sections of the blade.

For the Power Curve Task, the blades are optimized for a low wind speed of 4 m/s. This ensures that the turbine can produce power at the lowest windspeed of the task, 5m/s. The chord length calculations and the airfoil selection are completed with Airfoilbook 5, a python program our team developed this year. The new code is based in blade element momentum theory (BEM) and quickly calculates axial and tangential induction factors to determine optimum chord lengths as well as inflow angles and velocities. The inflow velocities and chord lengths are then used to determine the Reynolds number and Mach speed of the airflow at each section of the blades. The performance of each airfoil is analyzed by sending the Reynolds and Mach speed to Xfoil 6.99 and running a polar analysis to find the coefficients of lift and drag for a range of attack angles. Multiple instances of Xfoil are processed at once using parallelization which allows it to analyze all 1600 airfoils available in University of Illinois Urbana-Champaign (UIUC) airfoil database in less than 20 minutes. The airfoil that produces the design coefficient of lift with the lowest coefficient of drag is selected for the blade. Finally, the blade twist is calculated with inflow angle and optimum angle of attack for each blade section.

The Selig-Donovan and Selig-Giguere airfoil families were used because they were designed for wind turbines at low Reynolds number airflow. The chosen airfoil for our turbine blade was the SD2030. The last step before manufacturing is analyzing the blades performance in the newly released Qblade CE, to take advantage of Qblade's more precise BEM analysis and produce the coefficient of power vs TSR graph seen below [Figure 6].

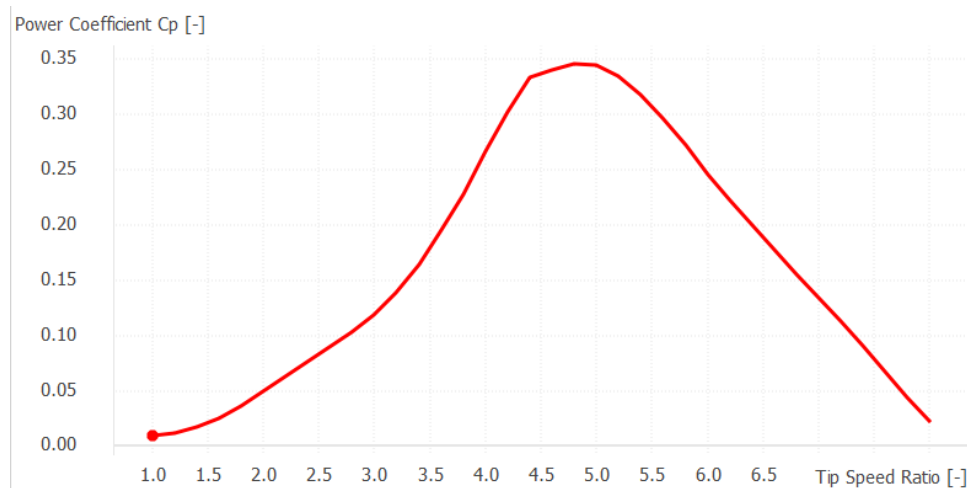


Figure 6: C_p vs. λ (TSR) with DTU Poly BEM, Prandtl Tip Loss, and 3D Correction

Satisfied with the performance, the blades are modeled in SOLIDWORKS and printed using an ultraviolet (UV) resin Liquid Crystal Display printer which has a much higher resolution than traditional FDM printers [Figure 7]. This is useful for accurately producing the airfoil geometry needed for a high-performance turbine blade. Once the blades are printed, all uncured resin is removed with isopropyl alcohol and the blades are cured for an additional 3 minutes under a UV lamp. This step increases the tensile strength of the resin to 49 MPa. Utilizing the QFEM tool in QBlade CE allows us to calculate the stress our blades will undergo is 2.06 MPa under static loading conditions. The additional curing process, while increasing tensile strength, also increases the brittleness of the blades. Initial blades had very fragile trailing edges that were prone to chipping during assembly. Chipping was prevented by making the trailing edge a minimum thickness of 0.15mm which is the cause of the squared-off trailing edge.

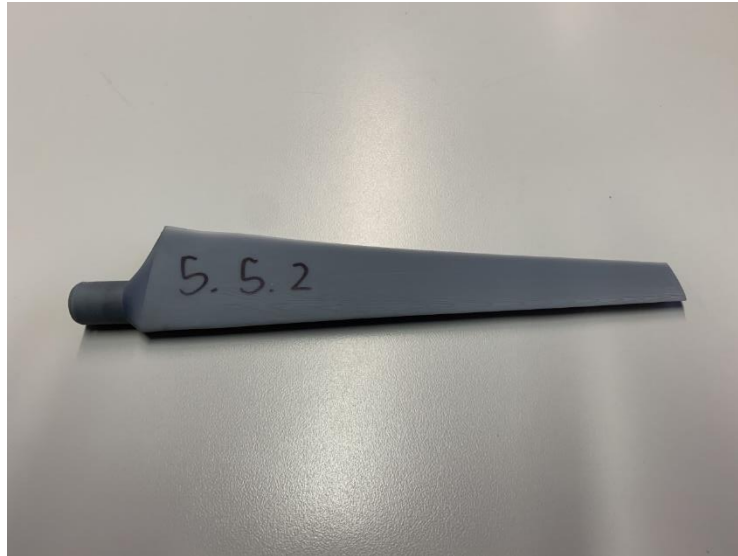
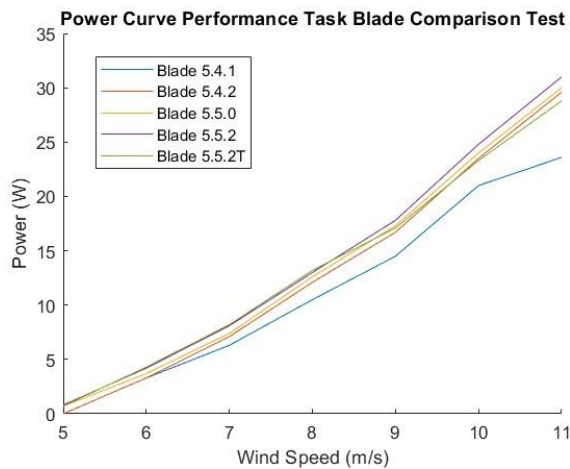


Figure 7: Final competition blade design (5.5.2)

After finalizing our design, we tested in the wind tunnel to confirm our simulation results. We tweaked the airfoil selection process to improve the blades between prototypes. The following graph and chart show the comparison of power output at various wind speeds for several different iterations of our blades. We calculated our Power Curve Performance Task score for each blade to get an accurate grasp on the blades expected competition results. Our highest score was 37.16 with blade design 5.5.2, surpassing the team’s past competition performance [Figure 8].



Blade Power Curve Performance Task Scores	
Blade Name	Score
5.4.1	29.49
5.4.2	33.48
5.5.0	35.31
5.5.2	37.16
5.5.2T	36.44

Figure 8: Power Curve Performance Task blade comparison test results

Generator Selection

To select our generator, our team conducted testing to determine a suitable fit for our system. Performance during the *Power Curve Performance Task* was the most important selection criteria. Our team selected two brushless DC generators with differing rated power and RPM to test. Upon testing, a 48V 6000RPM generator scored 25.57 on a *Power Curve Performance Task*, while a 24V 4000RPM generator only scored 22.15 [Figure 9]. Our team selected the DB42C01 48V 6000RPM brushless DC

generator for our turbine. While the selected generator has a rated voltage of 48V, during testing, the voltage never exceeded 12V. Additional voltage regulation to stay under the competition limit of 48V will not be necessary due to our generator choice. The selected generator also boasts a built in Hall-Effect sensor which our team uses to measure RPM of the turbine. The built in Hall-Effect sensor reduces the needed space inside of the nacelle by eliminating the need for an external RPM measurement device.

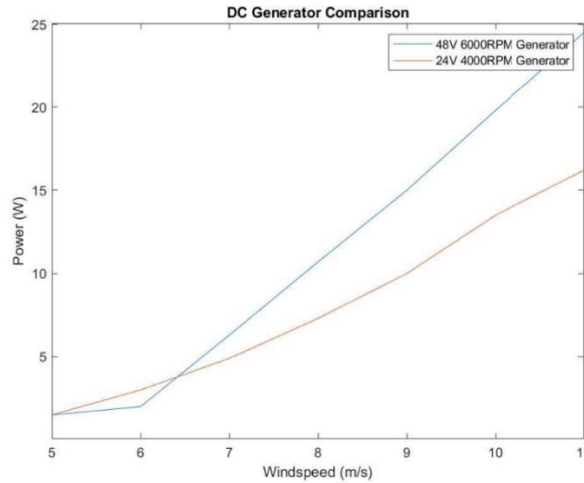


Figure 9: Generator Testing Power Curve

Turbine Side

The turbine-side printed circuit board (PCB) was designed with power efficiency and simplicity in mind. The board contains circuitry for a rectifier, a low pass filter, PCC disconnect detection, linear actuator communication, and a Hall-Effect sensor. The board also has buck and buck/boost converters to power said circuitry and an idle power consumption of approximately 0.7W. A one-line diagram outlining our electrical system’s main power paths can be seen in Figure 10.

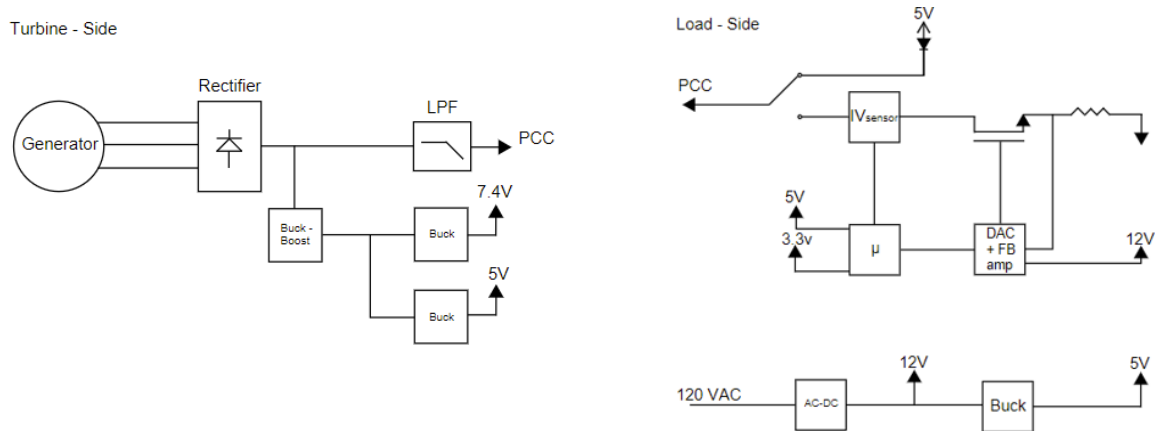


Figure 10: Electrical System One-Line Schematic

The turbine-side board contains 9V, 7.4V, and 5V power rails. The 5V rail powers optical isolation circuitry, the hall effect sensor, and a half to full-duplex converter IC for the linear actuator. The 7.4V rail powers the linear actuators. The 9V rail acts as an input to parallel buck converters whose outputs

are the 7.4V and 5V rails. The 9V rail is created by a wide input range (2.9-30V) Pololu DC to DC buck/boost converter.

Initially, our active rectifier displayed potential during breadboard testing. However, once the design was integrated into our final PCB, it failed to operate correctly and consumed more power than a conventional diode bridge rectifier. Nevertheless, we were able to convert our system into a three-phase diode bridge rectifier design, as we had anticipated the possibility of a failure of this kind and designed this part of our board to be adaptable.

Our rectified voltage is filtered through two bypass capacitors and a series inductor to reduce voltage and current ripple at the PCC. During testing, we verified through our data acquisition system that our power fluctuation remained below what is acceptable during the *Power Curve Performance Task*.

This year, we sought to simplify our method of detecting a PCC disconnection. In previous years, we've used an IV sensor IC on the turbine side board in order to know the exact voltage on the turbine side of the PCC. This year, we reduced the complexity down to a simple Schmitt-trigger comparator circuit that would be driven high or low when the PCC voltage went above or below a certain voltage. However, during testing, we realized that even a comparator was unnecessarily complicated. Since the comparator only had power when the turbine-side board had power, the input threshold voltage became irrelevant. Instead, we decided to ground one channel of an inverting buffer which drives an optocoupler connected to the load-side microcontroller. When the turbine-side voltage is high, the buffer is on and the microcontroller sees a logic low, otherwise, the buffer is off and a pull-up resistor on the optocoupler output creates a logic high.

Our generator's Hall effect sensor requires 5V to be powered and has three output signals, one for each phase of the generator. Since only the frequency and not the relative phase of the output signal is relevant to our RPM calculation, any one of these three could be used. The sensor output is open drain and uses a 4.7k Ω pull-up resistor. The signal is optically isolated and sent to the system's microcontroller where the frequency is measured and multiplied by a constant factor which converts it to the generator shaft RPM.

During a PCC disconnect safety state, for the linear actuators to fully pitch the blades before power is lost, a large amount of capacitance was added to the 9V and 7.4V rails. The 9V rail contains 40 and 15mF, 10V capacitors. The 7.4V rail also has a 40mF, 10V capacitor attached to it. The LC filter contains 2200 and 3300uF capacitors both rated for 25V. This totals 6.46J of energy storage on the turbine-side board.

Load Side

Our load-side PCB contains a controlled current sink MOSFET load, a load IV sensor, a PCC relay, opto-isolators for communication with the turbine-side board, and a Teensy 4.1 microcontroller which runs our entire electrical system's state machine. The load-side PCB is powered by 120VAC and has an idle power consumption of approximately 3.3W, the majority of which is consumed by the enclosure's exhaust fan.

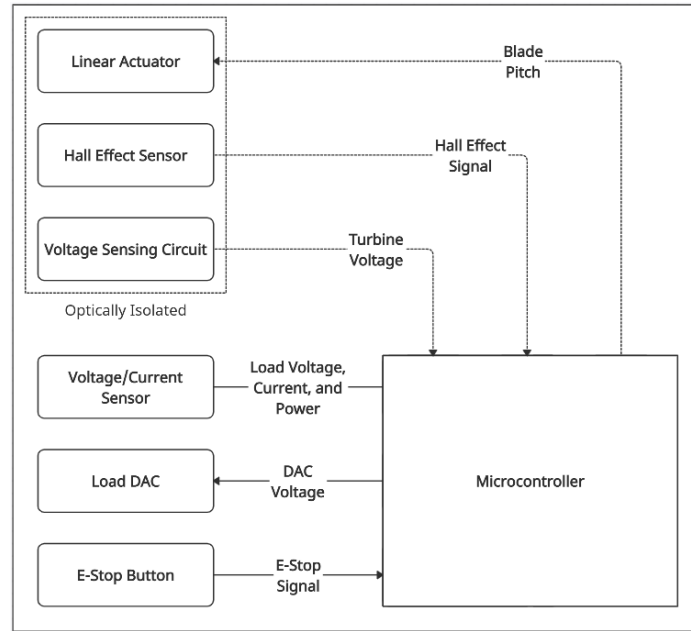


Figure 11: Load-Side Block Diagram

Our team made the decision to use a singular microcontroller on the load-side board instead of a microcontroller located on either side of the PCC. For one, we believed it was most logical to have our central processing unit located on a board which would always have consistent power during testing. Additionally, last year, communicating with another microcontroller on the turbine-side board proved difficult during conditions of low or unstable turbine power. While an undervoltage-lockout circuit would most likely help prevent microcontroller brownouts, this could mean that our turbine-side electronics would be entirely inoperative during low power conditions. The team decided that turbine-side ICs would interface directly with the load-side microcontroller over optically isolated channels instead of with an on-board microcontroller.

Early in the first semester, our team decided to prototype a load architecture which would primarily control load current. While our team had great success with a variable resistance load last year, our variable current design sought to improve the load by increasing the absolute range of load impedances, increasing the precision of impedances that the load can take on, and decreasing the complexity of accompanying circuitry. Figure 12 shows a schematic of the principal design.

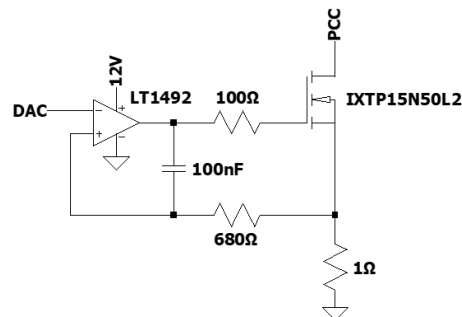


Figure 12: Fundamental Load Schematic

In theory, once the DAC voltage is set, negative feedback to the Op-Amp will adjust the MOSFET gate voltage in order to maintain a constant voltage across the source resistor. This results in a constant

current through MOSFET and source resistor. The maximum allowable current is approximately equal to the maximum DAC voltage divided by the value of the resistance to ground attached at the source of the MOSFET (1Ω in Figure 12). The load N-FET was chosen partially because of its high current rating, but mostly because it was intended to operate in its linear region, which is necessary for the design. The passive values in the feedback path were found through trial and error after the prototype was breadboarded. Until the optimal passive values were found, the load would usually experience large and slow oscillations in current. The final prototype, however, experienced current oscillations of less than 10mA when connected to a constant load voltage and constant DAC voltage. After seeing benchtop success, a variation of the design was added to the final schematic, which can be seen in Figure 13.

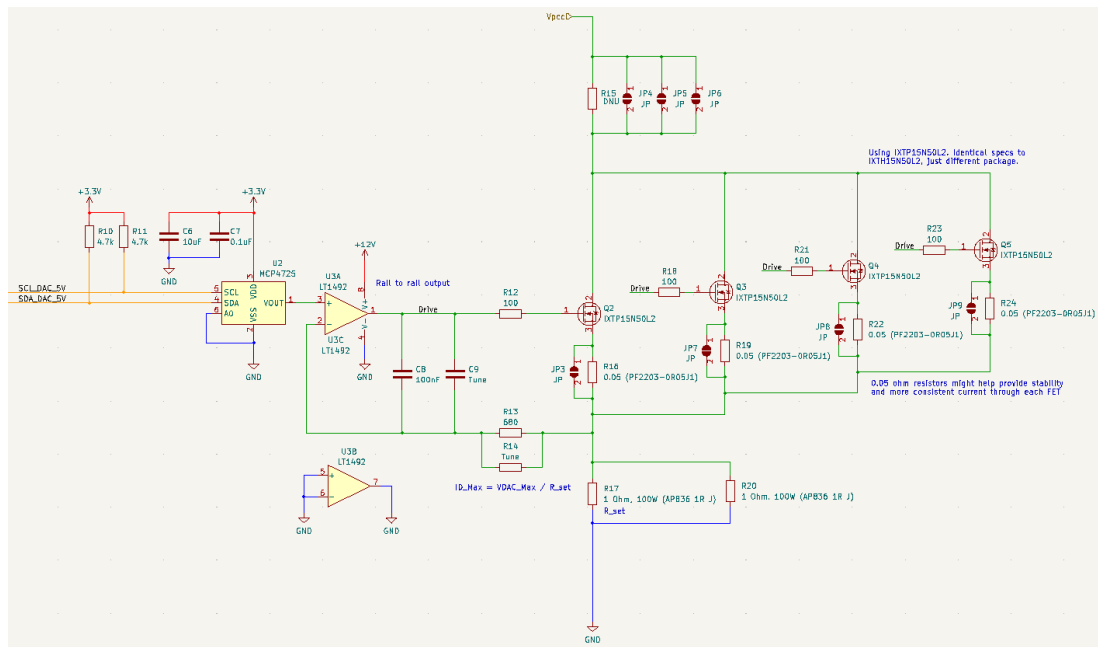


Figure 13: Final Load Schematic

The largest change between the final design and prototype was the number of MOSFETs used. By putting three additional MOSFETs in parallel, the power dissipated by each one is quartered. In making this change, we wanted to prepare for the possibility of performance changes as well. We added additional through-hole footprints in parallel with the passive feedback components critical to reducing oscillation in case those values needed tuning. We also added additional spots for resistors on the drains and sources which would further reduce the amount of power dissipated across each FET and possibly help alleviate current imbalances between the FETs. Testing of the design with a benchtop power supply was primarily successful without the need of additional tuning passives or resistors.

However, when the new load was finally tested with a turbine in our wind tunnel, we encountered some unexpected results. Last year, we saw our generator respond well to a specific resistance during the *Power Curve Performance Task*. So, this year, we hypothesized that the same would be true for a specific current. When trying to pull constant current from the generator at a fixed wind speed, the turbine would oscillate greatly in RPM shortly before the RPM fell to near-zero due to overloading. We tried to remedy this issue by instead writing a perturb and observe algorithm which would attempt to continuously respond to the generator and find an optimal current. This algorithm sometimes kept the turbine running for longer, but still resulted in large RPM and power oscillations. Our postulation is that

any control algorithm which attempted to find an optimal current ended up overloading the generator whenever there was a decrease in generator voltage due to transience or mechanical noise. If the system tried to maintain current during a voltage drop, the equivalent resistance of the load would be decreased, which resulted in a positive feedback loop further decreasing the RPM and generator voltage. To fix this issue, a resistance-based algorithm was developed. This program aimed to make our load look more like a resistor than a current sinking load by maintaining a voltage to current ratio. This adjustment showed immediate improvement to our system.

All power produced by our turbine is dissipated in the form of heat. Both the power MOSFETs and resistors of our load have aluminum heatsinks fastened to their TO-220 package. Our heat sink system can dissipate over 200W of power at room temperature. To maintain stable temperature inside the box, an exhaust system has been designed. A 19 CFM exhaust fan coupled with a filtered air inlet provide ample heat rejection for the system while maintaining NEMA1 standards.

In our load power path is an INA260 current and voltage sensor IC. This chip is located right before our MOSFET load and informs our microcontroller of the current through and voltage across our load over an I2C bus. This information allows us to perform the current and voltage ratio matching described above in order to make our load appear more like a resistor. It also informs our system during the *Control of Rated Power and Rotor Speed Task* by calculating power with voltage and current data.

The load-side of the PCC is connected to the common pin of a relay controlled by the microcontroller. The normally closed path of the relay connects to the IV sensor and MOSFET load previously described. The normally open path, however, is connected to the load-side board's 5V rail through a diode. The microcontroller can flip this relay to the normally open path in order to provide power to the turbine-side board when initializing cut-in pitch or exiting safety states. The diode protects the 5V rail in the event the path is connected when the generator is producing a higher voltage. The only rework performed on this section of the board was the addition of a current limiting resistor in series with the diode. When powering the turbine-side electronics through this path without the current limiting resistor, the 5V rail would momentarily sag and brownout the microcontroller.

Optical isolation circuitry for communication between the load and turbine-side board appears on the load-side PCB [Figure 14]. Isolation is done with two-channel, high-speed optocouplers. To ensure adequate current, the recommended inverting buffer ICs drive the LED side of the optocouplers. This provides two logic inversions, meaning that the output of the optocouplers is the same logic as the input of the buffers. The load-side board contains isolated ground and 5V rail planes that connect to the turbine-side board, meaning certain ICs will only be powered and operational when the turbine-side board has power.

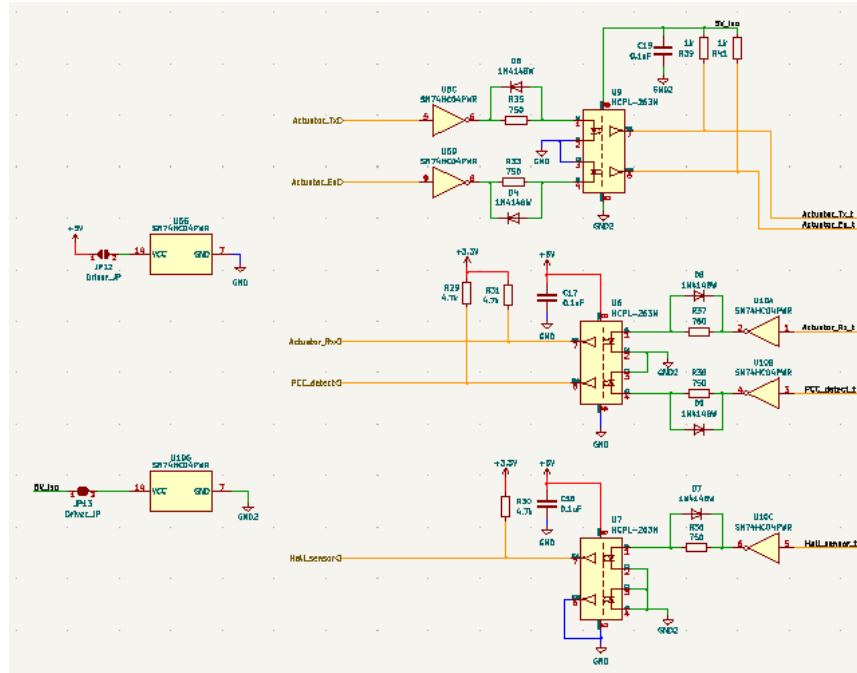


Figure 14: Optical Isolation Schematic

We decided that our emergency stop switch should be located on the load-side board because it always has power. If it was located on the turbine-side board, we would only be able to use the emergency stop when the turbine-side board had enough power to facilitate communication. A 470 Ω pull-up resistor connected to the microcontroller and competition provided switch enables emergency stop signal detection. When closed, there will be approximately 7mA through the switch, and the microcontroller will read a logic low. When open, the current through the switch will naturally be 0A, and the microcontroller will read a logic high, causing the turbine to shut down.

The load-side board contains 12V, 5V, and 3.3V rails. The 12V rail comes from our AC to DC converter which has a 120VAC wall-plug input. The 12V rail is used by the MOSFET load gate driver Op-Amp, exhaust fan, and 5V buck converter. The 3.3V rail is provided by an integrated LDO on the Teensy 4.1 microcontroller. ICs throughout the load board utilize the 3.3V and 5V rails.

Electrical Systems Manufacturing

PCBs for both the turbine and load-side are manufactured by JLCPCB and contain a combination of surface mount and through-hole components. The assembly process begins with the placement of surface mount parts onto the boards. This is accomplished by securing footprint stencils onto the boards, applying solder paste across the stencils, removing the stencils, placing the components onto the boards, and then baking the boards in a reflow oven. After the boards have cooled down, each chip is inspected under a microscope to ensure that reflow is adequate. In some cases, minor additional rework is required to reposition chips or remove solder beads that may be shorting neighboring pins. The remaining through-hole components are manually soldered in place.

To protect our PCBs with NEMA1 standards, we have chosen to use polycarbonate enclosures due to their malleability [Figure 15]. Our team has utilized drill and rotary tools to create holes for the installation of cable passthroughs and a heat rejection system. Our enclosure manufacturing process ensures that each PCB can be easily removed during the subassembly testing.

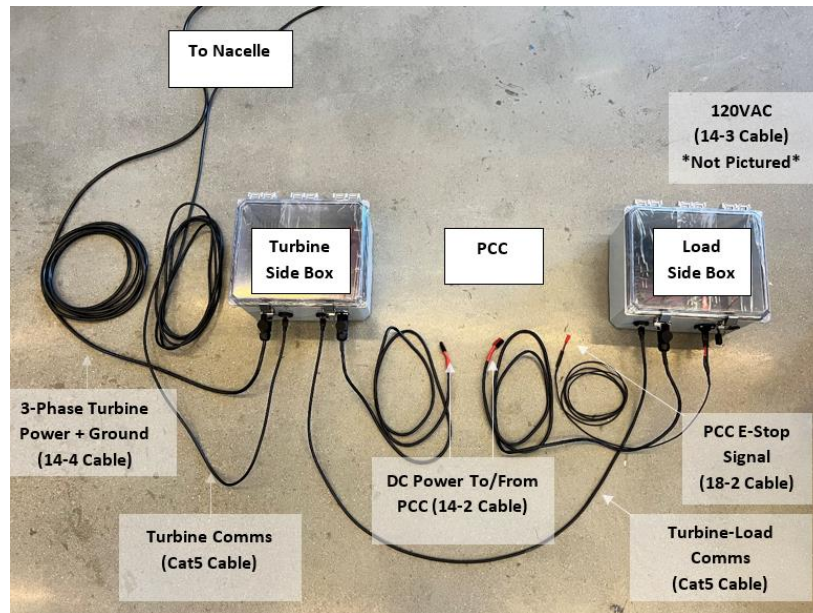


Figure 15: System Cable Map

Software

Software development for our team this year started with smaller code blocks for individual electrical subsystems. While prototyping, code blocks for our linear actuator, MOSFET load DAC, IV sensor, and Hall-Effect sensor were made. For the Teensy to communicate with our linear actuator, MOSFET load DAC, and IV sensor, each part required a library provided by the manufacturer. Once these were downloaded, test code was run to confirm that each part was operational. The Hall-Effect sensor code, however, was entirely original because we simply count and take a moving average of the sensor's output frequency to calculate generator RPM. Each of these parts required some minimal amount of additional electrical hardware in order to test operation. The linear actuator code was tested with our team's old turbine-side board because it was populated with a necessary half to full-duplex digital communication buffer IC. The MOSFET load DAC code was tested with a small breakout board manufactured by Adafruit which was populated with the desired DAC. The IV and Hall-Effect sensor code was also tested with the team's old electronics which contained the desired ICs and necessary pull-up resistors.

After electrical subsystem software was developed, software components could be integrated together. Components were brought together in Arduino IDE utilizing GitHub as a repository. This phase of the software development process corresponded with the completion of our team's PCB fabrication. This allowed all the electrical subsystems to be controlled by a single Teensy 4.1 microcontroller which facilitated the integration of subsystem code.

After confirming that individual software components did not negatively interfere with each other, a full program for competition was developed. This program development began with the building of user interface in the form of the Arduino serial monitor. This interface displays all microcontroller data and allows the user to change variables in the software. This interface allows our team to view and gather data for testing purposes. Finally, the state machine to run our system was built.

State Machine Operation

Our team's turbine operates using a state machine control model with states designed for individual turbine testing tasks [Figure 16]. Separating each turbine testing task into a state allowed for a more efficient design process. These states were first tested individually before the transitions and state

machine were tested. From our experience, transitions between states are the most crucial part of the system.

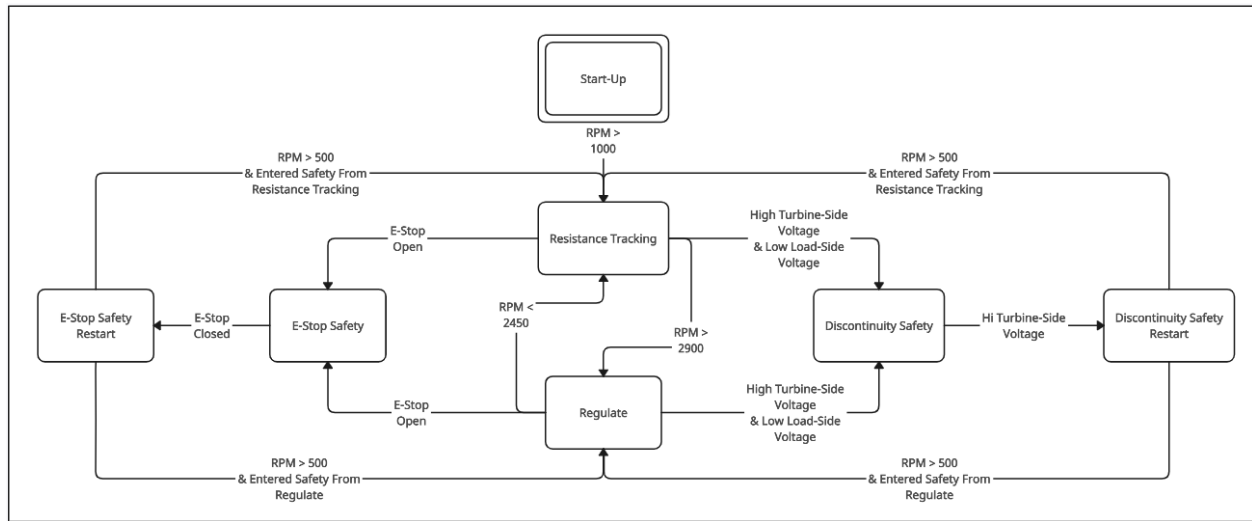


Figure 16: State Diagram

- *Start-Up State*

The Start-Up state is the default state of the system and is only operated during windspeeds below 5 m/s. This state sets the pitch of the blades to the optimal cut-in pitch and allows no current to flow into our load. These two conditions maximize RPM which helps the generator overcome static friction. Once our turbine has surpassed 1000 RPM, it will transition to the Resistance Tracking state.

- *Resistance Tracking State*

Our system remains in the Resistance Tracking State during the entirety of the *Power Curve Performance Task*. During this state, our blade angle and effective load resistance are set to fixed values that produced the best *Power Curve Performance Task* score recorded during testing.

- *Regulate State*

The Regulate State is where the system operates during both the *Control of Rated Power and Rotor Speed Task* and the *Durability and Foundation Success Tasks*. RPM of our turbine is used to determine when to enter and leave the state. Our system remains in this state from 11 m/s to 22 m/s. This state uses blade pitch as the primary regulation mechanism and effective load resistance as a secondary control mechanism. The setpoints that our team regulates to are the maximum RPM and Power at 10.5 m/s. To regulate RPM, our system utilizes blade pitch and a dynamic step-size algorithm. The algorithm analyzes the difference between our desired RPM and the current RPM to determine how large an adjustment is needed. Once the adjustment is made, there is a settling time to allow for the change to take effect and the process is repeated. Fine power regulation is controlled by our MOSFET load. This regulation is also a dynamic step-size algorithm very similar to the RPM regulation algorithm. As the wind speed increases, our blades feather more and our load increases its effective resistance. This minimizes mechanical and electrical stress on our system. Successful operation of this state can be seen from the data presented in Figure 17.

- *E-Stop Safety State*

The E-Stop Safety State allows our system to shut down during the e-stop portion of the *Safety Task*. This state is entered upon the opening of the e-stop button contacts. Immediately upon entering the

state, power is provided to the turbine-side board through the PCC and the blades are fully feathered to halt rotation. Next, our system waits for the e-stop button to close.

- *E-Stop Safety Restart*

This state allows our system to smoothly come back up to speed when exiting the E-Stop Safety state upon the signal that the button has closed. Once the state is entered, the blades are pitched to their operational angle and the system is allowed time to spin up. Once sufficient RPM is achieved, the state machine returns to the state the system was in when the e-stop button was pressed.

- *Discontinuity Safety State*

The Discontinuity Safety State allows our turbine to shut down during the discontinuity portion of the *Safety Task*. Entrance to this state is signaled by a high voltage on the turbine-side board and a low voltage on the load-side board. This signals that there is a discontinuity at the PCC. Upon entering the state, the blades are fully feathered. The power necessary for this action is supplied by capacitors on the turbine-side board. After a waiting period to ensure the capacitors have discharged, our load-side board attempts to supply power to the turbine-side board. A reconnection has occurred when the power is successfully supplied to the turbine-side board and a high voltage on the turbine-side is seen. Once a reconnection has occurred, the system transitions to the Discontinuity Safety Restart state.

- *Discontinuity Safety Restart State*

The Discontinuity Safety Restart State transitions from a discontinuity safety task back to normal operation. Upon entrance to the state, the blades are pitched to their operational pitch which allows the system to gain speed. Once the system is at operating speed, the state machine is returned to the state the system was in when the disconnect occurred.

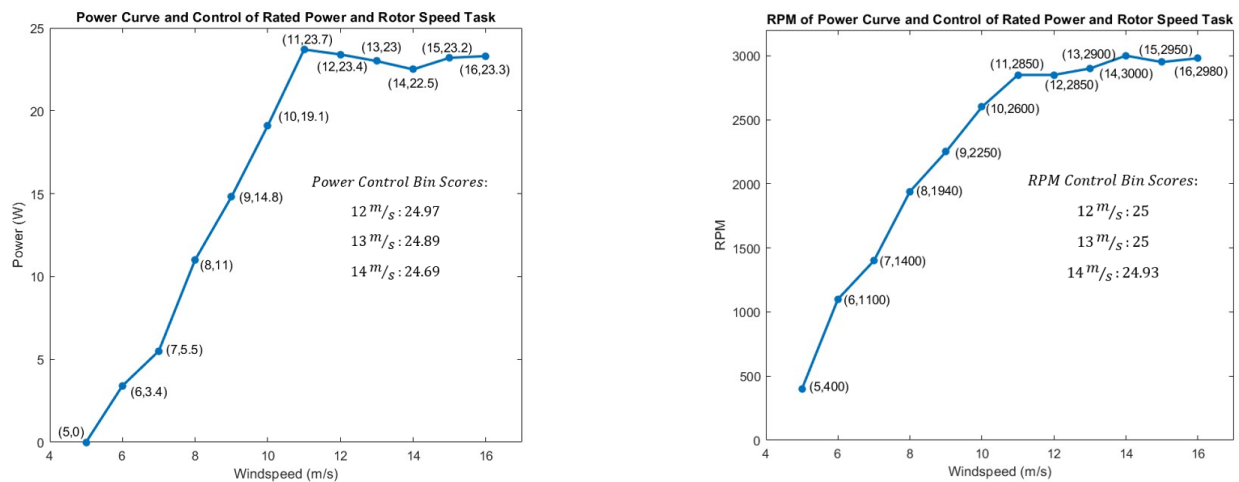


Figure 17: Power Curve and Control of Rated Power and Rotor Speed Task Test Results

Final Turbine Assembly

In an effort to minimize installation time at the wind tunnel, all subsystems that can be assembled will be assembled prior to our provided installation time. The nacelle assembly is the primary component that can be fully constructed before installation. This assembly process includes: mounting the generator inside the nacelle, fastening the active pitch mechanism to the generator, attaching the tailfin, and closing the hatch atop the nacelle. The foundation, electronics, and combined nacelle assembly will require installation during our allotted installation time. These systems were designed for ease of installation as time is an important aspect of the process. After our foundation is installed, the rest of the on-site assembly process takes no more than five minutes. To ensure proper installation on-site, our team has developed an assembly and commissioning checklist seen below.

Assembly and Commissioning Checklist

Assembly and Commissioning Step	Initiating Team Member Initials	Verifying Team Member Initials
Attach the foundation installation tool to the top of the foundation tubing with set screw	JM	JL
Feed the turbine power and the communication cables through the foundation tubing	JM	JL
Set the foundation into the tank and turn the tool clockwise until the foundation is level with the top of the tank	JM	JL
Check foundation for level	JM	JL
Unscrew the set screw, remove the foundation installation tool	JM	JL
Ask the judges to move the tank under the tunnel and install the stub	JL	MB
Feed the turbine power and the communication cables through the turbine tower	DP	MB
Place the tower on the stub, tighten the wingnuts to secure the tower to the foundation	RS	JL
Connect the communication and the power cable from the nacelle to their corresponding cables	DP	MB
Carefully feed the cables back into the tower and place the nacelle on the press-fit bearing at the top, the nacelle should push down firmly and sit flush with the bottom of the bearing	DP	MB
Orient the nacelle in the upwind direction	JL	RS
Connect the power and communication cables from the turbine to the turbine control box	DP	MB
Connect the DC power cable for the turbine-side box to the PCC	DP	MB
Connect the communications cable from the turbine control box to the load side box	DP	MB
Connect the DC power cable from the PCC to the load-side box	DP	MB
Connect the power cable from the load side box to 120VAC	DP	MB
Connect the emergency stop cable from the load-side box the PCC	DP	MB
Ensure the heat rejection fan is running in the load-side box	DP	MB
Verify active pitch system has actuated to cut-in pitch	DP	JL

References

- [1] J. Burton, N. Jenkins, and D. Sharpe, "Wind Energy Handbook," Chichester, West Sussex, UK: John Wiley & Sons, Ltd, 2001.